Biosensors and Bioelectronics 95 (2017) 152–159

Contents lists available at ScienceDirect

Biosensors and Bioelectronics

journal homepage: www.elsevier.com/locate/bios

# Portable aptamer biosensor of platelet-derived growth factor-BB using a personal glucose meter with triply amplified

Lu Hong[a,b,c], Fu Zhou[a,b,c], Dongmin Shi[a,b,c], Xiaojun Zhang[a,b,c], Guangfeng Wang[a,b,c,d,*]

[a] Key Laboratory of Chem-Biosensing, Anhui province, PR China
[b] Key Laboratory of Functional Molecular Solids, Anhui province, PR China
[c] College of Chemistry and Materials Science, Center for Nano Science and Technology, Anhui Normal University, Wuhu 241000, PR China
[d] State Key Laboratory of Chemo/Biosensing and Chemometrics, Hunan University, Changsha 410082, PR China

ARTICLE INFO

*Keywords:*
PDGF-BB
Catalytic and molecular beacon
8–17 DNAzyme
Personal glucose meter

ABSTRACT

Sensitive and rapid detection of platelet-derived growth factor BB (PDGF-BB), a cancer-related protein, could help early diagnosis, treatment, and prognosis of cancers. Although some methods have been developed to detect PDGF-BB, few can provide quantitative results using an affordable and portable device that is suitable for home use or field application. In this work, we report the first use of a portable kind of personal glucose meter (PGM) combining a catalytic and molecular beacon (CAMB) system with a cation exchange reaction (CX reaction) for ultrasensitive PDGF-BB assay. It realized the amplification of the detection in three ways, including greater aptamer payload on nanoparticles, CX reaction releasing thousands of $Zn^{2+}$ and the cycle by the catalyzing cleavage of 8–17 DNAzyme. In the process, with the addition of PDGF-BB into the aptasensor, the specific recognition between aptamer and protein was initiated resulting in the combination of ZnS NNC for further CX reaction to release thousands of $Zn^{2+}$, which could cleave the substrate DNA in the CAMB system realizing multiple cycle. The cleaved DNA fragment was designed with invertase-labeled could convert sucrose into glucose which could be detected and quantified by PGM accompanying with the change of color of the control window from yellow to green. The enhanced signal of the PGM has a relationship with the concentration of PDGF-BB in the range of $3.16\times10^{-16}$ M to $3.16\times10^{-12}$ M, and the detection limit is 0.11 fM. Moreover, the catalytic and cleavage activities of 8–17 DNAzyme can be achieved in solution; thus, no enzyme immobilization is needed for detection. The triply amplified strategy showed high selectivity, stability, and applicability for detecting the desired protein.

## 1. Introduction

Platelet-derived growth factor-BB (PDGF-BB), an important cytokine in serum, plays a vital role in regulating cell growth and division. It is a necessary protein for increased healing coupled with fibroblast activation and granulation tissue formation in the treatment of some human chronic dermal wounds (Pierce et al., 1995). Because it is close to several horrible diseases such as atherosclerosis, fibrosis and often overexpressed in human malignant tumors serving as an indicator for tumor angiogenesis (Clarke et al., 1984), the recognition and quantification of PDGF-BB are of particular significance in biomedical fields. Until now, various methods have been applied in PDGF-BB determination, such as fluorescence (Qiu et al., 2011), chemiluminescence, colorimetry (Tang et al., 2012) and electrochemistry (Wu et al., 2010). Most of these methods possess high sensitivity and selectivity, but relatively expensive equipment and trained operators are often needed, which made their application limited in remote areas. Therefore, it is highly desirable to develop an easy and portable sensor for sensitive determination of PDGF-BB.

The development of portable sensors for rapid, on-site and cost-effective detection of a broad range of targets has long been sought, because such sensors have the potential to revolutionize scientific research, environmental monitoring and personal healthcare in urban areas in developed countries as well as rural areas in developing countries (Daar et al., 2002; Martinez et al., 2007; Fan et al., 2005; Xia et al., 2010; Zhang et al., 2002; Giepmans et al., 2006; Wegner et al., 2007; Murray et al., 2008; Wang et al., 2010; Favier et al., 2001). Despite their great promise and many years of investigation, only a limited number of sensors are commercially available to the public at present. Perhaps the most successful example of the portable sensor is the personal glucose meter (PGM) (Clark et al., 1962; Montagnana et al., 2009), which is widely available in stores and has either saved or

* Corresponding author at: Key Laboratory of Chem-Biosensing, Anhui province, China.
*E-mail address:* wangyuz@mail.ahnu.edu.cn (G. Wang).

http://dx.doi.org/10.1016/j.bios.2017.04.023
Received 26 December 2016; Received in revised form 31 March 2017; Accepted 18 April 2017
Available online 19 April 2017
0956-5663/ 

improved the quality of lives of millions of diabetic patients worldwide. The broad success of PGMs is largely due to its a great deal of advantages including the portable "pocket" size, cost effectiveness, reliable quantitative results and easy operation (Carroll et al., 2007). In the early stages of the development of PGM, the application of this successful portable sensor is limited in its single target (glucose) and its dynamic range of glucose (Clark et al., 1962; Montagnana et al., 2009). However, recently, researchers have developed various approaches to expand the application of PGM for the detection of different targets. For example, Xiang and Lu (Xiang and Lu, 2011, 2012a, 2012b, 2013) developed sensors to monitor a series of non-glucose targets by taking advantage of invertase-labeled functional DNAs and antibodies. Yan et al. (2013) reported a target-responsive "sweet" hydrogel combined with a commercial glucose meter for cocaine and adenosine triphosphate detection. Su et al. (2013) established a sensitive copper (II) sensor which combined the merits of PGM and click chemistry. In 2013, portable PGM has also been applied to detect PDGF-BB successfully by introducing invertase conjugates to secondary aptamer (Ma et al., 2014). However, due to the PDGF-BB exists at extremely low concentrations in living organisms, the routine aptameric methods hinder further development of PDGF-BB detection in real samples (Zhang and Zhang, 2012). Consequently, there still has been a major challenge to develop sensitive portable methods for the detection of PDGF-BB.

DNAzymes are nucleic acids that isolated from combinatorial oligonucleotide libraries by in vitro selection (Robertson et al., 1990; Breaker, 2000; Wilson and Szostak, 1999; Liu et al., 2009). DNAzymes are not only similar to protein enzymes, exhibiting high catalytic cleavage activity toward specific substrate, but also much more stable than protein enzymes, able to be denatured and restored many times without losing catalytic activity toward substrate and easily produced using a commercial DNA synthesizer (Liu et al., 2009). As one of the most interesting DNAzymes, $Zn^{2+}$-requiring 8–17 DNAzyme (Zhang et al., 2010; Lu et al., 2011; Jiang et al., 2015), is usually composed of a substrate strand and an enzyme strand. In the presence of $Zn^{2+}$, the specific cleavage of substrate strand is nicked, resulting in the substrate strand split into two fragments, one of which contains the signal molecules triggering the amplification. $Zn^{2+}$-requiring 8–17 DNAzyme exhibits many excellent characteristics, such as simple synthesis, good stability, easy labeling, and design flexibility, which enables $Zn^{2+}$-requiring 8–17 DNAzyme to be particularly attractive in sensing platforms as signal amplification elements for the design of aptasensor that are highly specific for a number of targets such as metal ions and small biological molecules (Liu et al., 2009; Zhang et al., 2011). Recently, by integrating an 8–17 DNAzyme with molecular beacon, a catalytic and molecular beacon (CAMB) amplified system has been reported, realizing the true enzymatic multiple turnover (one enzyme catalyzes the cleavage of several substrates) of catalytic beacons for amplified signal detection. The unique features make 8–17 DNAzyme integrated CAMB strategy very suitable for bioassay applications to amplify the signal.

Ion-exchange reactions based on place-exchanging the cations on the nanoscale ionic material with a different set of cations (Peng et al., 1998) have obtained great attention in chemical analysis, recovery of useful ions, materials synthesis and water purification. In chemical analysis, cation ion-exchange (CX)-based amplification is an effective amplification strategy to improve the sensitivity of assays. It was realized through the incorporation of metal ion with metallic nanoparticles to trigger large amounts of signal reporter unit which was usually from the newly produced ionic nanomaterials with diameter of a few nanometers. They can encapsulate thousands of the corresponding ions resulting in a large signal enhancement in this fast and gentle process. Due to the unique attributes of rapid kinetics at room temperature (orders of magnitude faster than in the bulk), the tuning of reactivity via control of nanocrystal size, shape, surface faceting and the avoidance of strong acids or corrosive oxidants, CX-based amplification has been employed as a convenient tool for sensitive detection of a variety of targets, such as DNA (Zhang et al., 2015a, 2015b, 2015c), microRNA (Li et al., 2009a), femtomolar proteins (Yao et al., 2012a, 2012b), telomerase (Wang et al., 2015), glutathione (Shi et al., 2013) and so on. Zhong's group has reported a series of work on cation-exchange-based fluorescence amplification (Li et al., 2009a, 2009b; Yao et al., 2011, , 2012a, 2012b, 2013). By exchanging nonfluorescent CdSe or ZnS NC clusters with $Ag^+$, $Ag_2Se$ NCs together with large amounts of the released $Cd^{2+}$ or $Zn^{2+}$ cations were formed. The generated cations can coordinate to metal-responsive fluorophores and further activate fluorogenic dyes. Due to each ZnSe NC, with a calculated diameter of 5.38 nm, contains 2051 Zn atoms (Kucuur et al., 2007), this CX-based amplification method exhibits remarkably high signal enhancement. Owing to the large amounts of $Zn^{2+}$ released through the simple CX reaction and as we know $Zn^{2+}$could specifically cleave the substrate strand in 8–17 DNAzyme system to amplify the signal, we were inspired to design a system combining the CX with $Zn^{2+}$-requiring-8–17 DNAzyme.

In this paper, we first report a novel triply amplified PDGF-BB aptasensor with the cost-effective portable PGM as readout. This triply amplified newly PGM platform couples the CAMB system with CX-based amplification. $Zn^{2+}$-requiring 8–17 DNAzyme was chosen as the catalytic unit due to its high catalytic activity and expanded functionality by the adoption of $Zn^{2+}$ as the cofactor. This strategy can significantly improve sensitivity in three ways. First, nanoparticles have large surface areas, providing greater aptamer payload. Second, each ionic nanocrystal can release thousands of $Zn^{2+}$ into solution by CX reaction. Third, one 8–17 DNAzyme can catalyze the cleavage of several substrates. Therefore, after the CX reaction, the CAMB system affords an amplified signal through cycling and regenerating the $Zn^{2+}$-dependent 8–17 DNAzyme to realize multiple enzymatic turnovers. The proposed portable aptasensor has been applied to detect PDGF-BB in clinical human saliva samples with satisfactory results. It is worth noting that the operating principle of this study could be extended as a general protocol for other targets of interest.

## 2. Experimental procedures

Materials, Apparatus and the electrochemical experimental process are in Supplemental information.

### 2.1. DNA-invertase conjugation

The conjugation procedure was similar to previous work with minor modifications (Xiang and Lu, 2011, 2012a, 2012b; Zhou et al., 2014). Briefly, 30 μL of 1 mM sDNA, 2 μL of 0.1 M buffer A, and 2 μL of 30 mM TCEP were mixed and kept at room temperature for 1 h. After that, the excess TCEP was removed by Amicon-3K using buffer A (0.1 M NaCl, 0.1 M sodium phosphate buffer, pH 7.4, without 0.05% Tween-20) for 3 times. Meanwhile, 1 mg of sulfo-SMCC was mixed with 400 μL of 20 mg/mL invertase in buffer A. After vortexing, the solution was placed on a shaker for 1 h at room temperature. Then, the mixture was centrifuged to remove excess insoluble sulfo-SMCC. The supernatant was washed 8 times by Amicon-100 K using buffer A. The above solutions of TCEP-activated sDNA and sulfo-SMCC-activated invertase were mixed and kept at room temperature for 48 h. To remove unreacted sDNA, the solution was purified by Amicon-100 K using buffer A over five wash cycles.

### 2.2. Synthesis of ZnS Nanocrystal Clusters (NCCs) and $Fe_3O_4$ NPs

The ZnS NCCs were synthesized by a hydrothermal approach, using thiourea $NH_2CSNH_2$ to control cluster growth. In a typical synthesis, 0.8 mmol of $Zn(Ac)_2{\cdot}2H_2O$ and 20 mmol of thiourea were dissolved in 20 mL of ultrapure water to form a clear solution after being stirred for 30 min at room temperature. The solution was then transferred into a

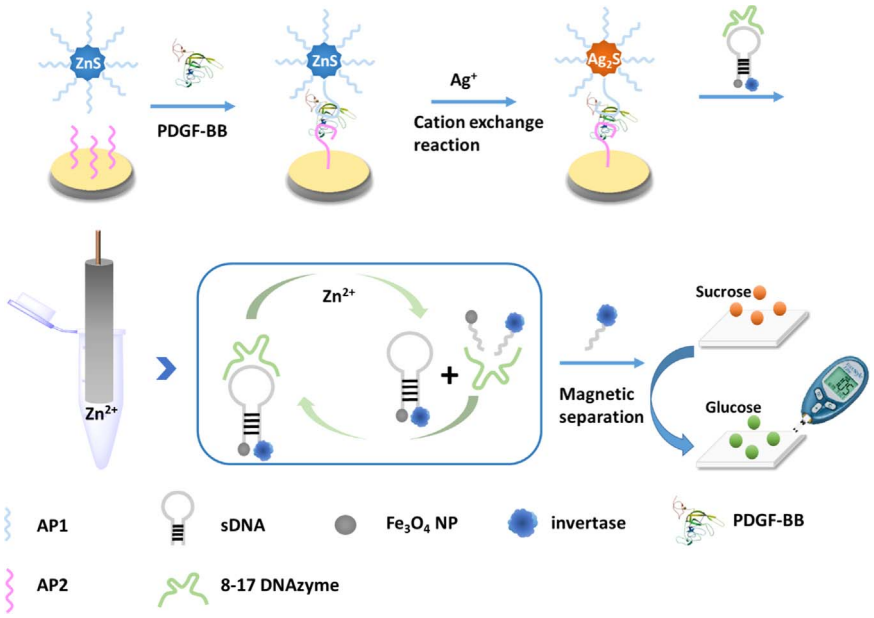


**Scheme 1.** Schematic of the portable aptasensor for PDGF-BB assay using the PGM as readout based on a triply amplification.

stainless steel autoclave (Parr Instrument Co., Moline, IL) with inner Teflon lining (40 mL) and maintained at 140 °C for 90 min in an Isotemp Oven (Fisher). After having been cooled to room temperature, the resulting white precipitate was harvested by centrifugation and washed twice with 20 mL of ultrapure water and once with 20 mL of ethanol. The aqueous stock cluster solutions used for portable aptasensor were prepared by washing the clusters with water and redistributing them in buffer A.

$Fe_3O_4$ microspheres were synthesized according to the literature (Deng et al., 2005). First, $FeCl_3{\cdot}6H_2O$ (1.35 g, 5 mmol) was dissolved in ethylene glycol (40 mL) to form a clear solution, followed by the addition of NaAc (3.6 g) and polyethylene glycol (1.0 g). After that, the mixture was stirred vigorously for 30 min and then sealed in a teflon-lined stainless-steel autoclave (50 mL capacity). Then, the autoclave was heated and maintained at 200 °C for 6–8 h, and allowed to cool at room temperature. Finally, the black products were washed several times with ethanol and dried at 60 °C for 6 h.

### 2.3. Bioconjugation of Zn NCCs and $Fe_3O_4$ NPs

Streptavidin was coupled to the amine-coated ZnS NCCs by EDC and sulfo-NHS. Twenty microliters of the stock ZnS NCCs (~2×1011 particles) were washed with 0.005% Tween-20 solution by centrifugation at 16.1k×*g* for 15 min before conjugation. The carboxyl group on streptavidin was activated by mixing 25 μL of 1 mg/mL streptavidin with 6 mg of EDC and 5 mg of sulfo-NHS dissolved in 1 mL of buffer A. After activation for 15 min, the residual EDC was quenched by 1 μL of 2-mercaptoethanol to prevent protein cross-linking. Then, ZnS NCCs were added to the activated streptavidin, and the mixture was gently vortexed for 3 h at room temperature. At last, the ZnS streptavidin conjugate was precipitated with centrifugation at 16.1×*g* for 12 min and resuspended in buffer A.

Streptavidin was coupled to the amine-coated $Fe_3O_4$ NPs by EDC and sulfo-NHS. Twenty microliters of the stock $Fe_3O_4$ NPs were washed with 0.005% Tween-20 solution by centrifugation at 16.1k×*g* for 15 min before conjugation. The carboxyl group on streptavidin was activated by mixing 25 μL of 1 mg/mL streptavidin with 6 mg of EDC and 5 mg of sulfo-NHS dissolved in 1 mL of buffer A. After activation for 15 min, the residual EDC was blocked by 1 μL of 2-mercaptoethanol to prevent protein cross-linking. Then, Fe3O4 NPs were added to the activated streptavidin, and the mixture was gently vortexed for 3 h at room temperature. At last, the $Fe_3O_4$ NPs streptavidin conjugate was precipitated with centrifugation at 16.1×*g* for 12 min and resuspended in buffer A.

### 2.4. Bioconjugation of ZnS-AP1 and sDNA-$Fe_3O_4$

A portion of 2 mL 1 mg/mL streptavidin coated $Fe_3O_4$ NPs solution were exchanged to buffer A twice and then dispersed in 2 mL buffer A. sDNA was added to the solution to achieve a final concentration of 5 μM, and the mixture was mixed on a roller for 30 min at room temperature. After that, the sDNA-$Fe_3O_4$ was separated from the mixture by a magnet. And then, the sDNA-$Fe_3O_4$ composites were further washed by buffer A for 3 times and separated as each portion of 50 μL with 1 mg/mL sDNA-$Fe_3O_4$ in buffer A.

A portion of 2 mL 1 mg/mL streptavidin coated ZnS NCCs buffer were exchanged to buffer A twice and then dispersed in 2 mL Buffer A. AP1 was added to the solution to achieve a final concentration of 5 μM, and the mixture was mixed on a roller for 30 min at room temperature. After that, the ZnS-AP1 composites were further washed by buffer A for 3 times and separated as each portion of 50 μL with 1 mg/mL ZnS-AP1 in buffer A.

### 2.5. Preparation of the modified electrode

The gold electrode (GE) (3 mm diameter) was carefully polished to a mirror-like finish with alumina powder of 0.3 and 0.05 mm, followed by sequential sonication for 10 min each in ultrapure water, ethanol and ultrapure water. Then it was dipped in freshly prepared piranha solution (98% $H_2SO_4$: 30% $H_2O_2$, 3:1 by volume) for 10 min and rinsed with ultrapure water thoroughly. The electrode was then scanned in 0.1 M $H_2SO_4$ between −0.2 V and 1.55 V at 100 mV/s until are producible cyclic voltammogram (CV) was obtained. Once completed, the electrode was washed with ultrapure water and dried under nitrogen. After pretreatment, the electrode was incubated with 10 μL of 1 μM AP2 solution (buffer B: 0.1 M NaCl, 0.1 M sodium phosphate buffer, pH 7.4, with 0.05% Tween-20) for 12 h at 4 °C. Then the resulting modified electrode was incubated with blocking solution (BSA, w/w, 0.25%) for 2 h to eliminate non-specific binding effects and block the remaining active groups. After every step, the electrode was thoroughly cleaned with buffer B and ultrapure water to prevent the non-chemisorption. Next, this electrode was immersed in PDGF-BB

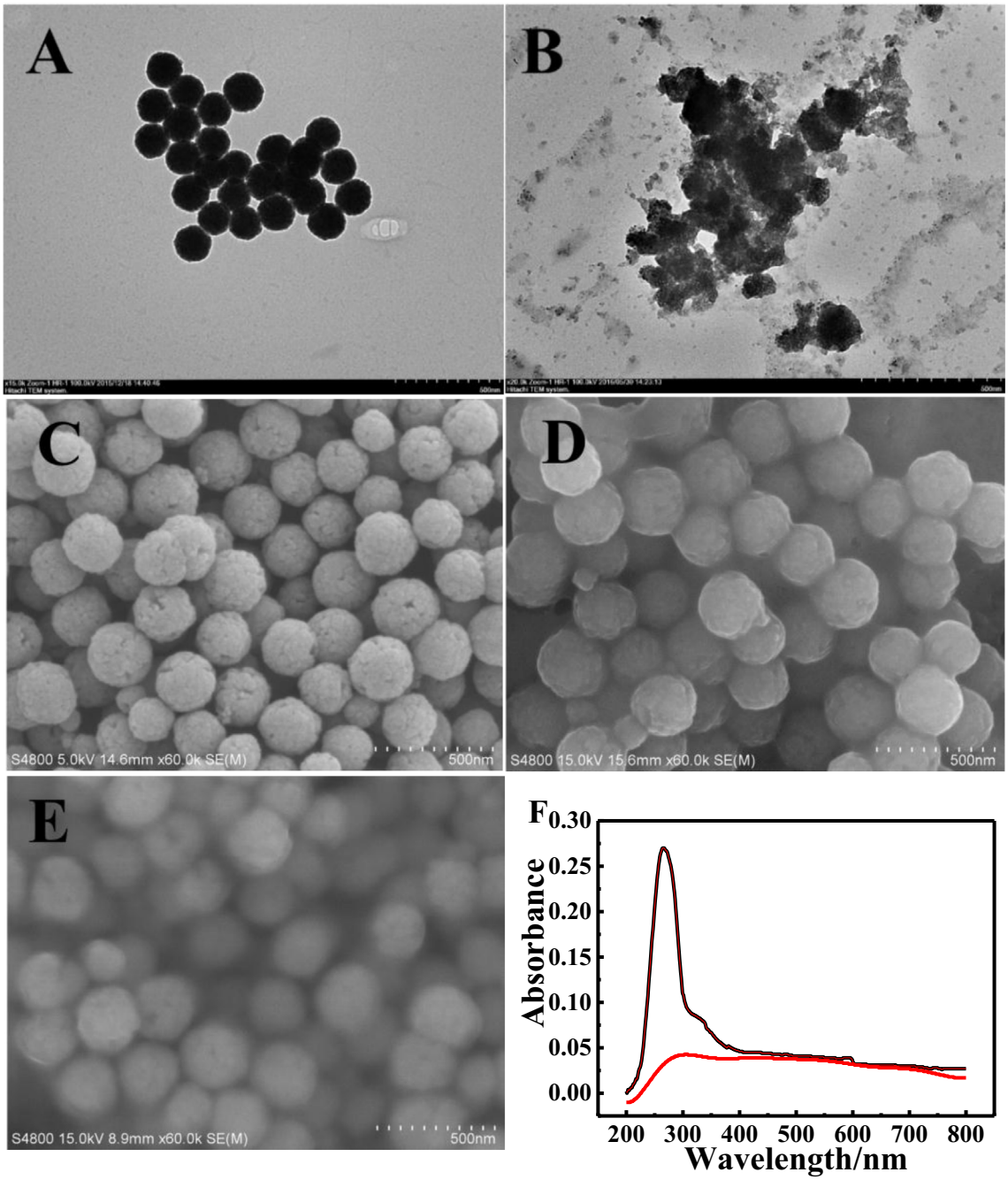


**Fig. 1.** (A) TEM image of ZnS NCCs (B) TEM image of ZnS-AP1(C) SEM image of the prepared $Fe_3O_4$ NPs (D) SEM image of the $Fe_3O_4$-SA nanoparticles (E) SEM image of the sDNA-$Fe_3O_4$ (F) UV–vis absorption spectroscopy of bare $Fe_3O_4$ NPs (a) and sDNA -$Fe_3O_4$ (b).

solution for 2 h at room temperature, rinsed with PBS to remove the nonspecifically bound PDGF-BB, and was then immediately soaked in 200 μL ZnS-AP1 conjugates for another 2 h at room temperature. Subsequently, the electrode was successfully modified with ZnS-AP1.

### 2.6. Procedures for PDGF-BB detection

CX was performed using a 14 μL solution of 1 mM $AgNO_3$ in 200 μL ZnS-AP1 solution for 10 min. Then, 150 nM sDNA and 75 nM 8–17 DNAzyme were added to the solution for 60 min at 37 °C. After that, sDNA with invertase were separated from the mixture by a magnet to remove the magnetic matter. Subsequently, 20 μL of the sucrose solution (1.0 M) was added into the solution carefully and kept at room temperature for 20 min. The enzymatic reaction generated glucose and then detected by the PGM. The data of PGM before and after the addition of PDGF-BB was collected for the quantitative analysis. All the measurements were repeated three times and the standard deviation was calculated for the error analysis. In the control experiment, the roles of PDGF-BB, AP1, ZnS-AP2 and $Ag^+$ were studied in the same process except the addition of the corresponding PDGF-BB, AP1, ZnS-AP2 and $Ag^+$.

## 3. Results and discussion

### 3.1. The principle of the portable aptasensor for PDGF-BB

The design principle for the portable and triply amplified quantitative detection of PDGF-BB is schematically described in Scheme 1. As shown in Scheme 1, there are four oligonucleotides involved in the present sensing system: AP1, AP2, sDNA and 8–17 DNAzyme. AP1 and

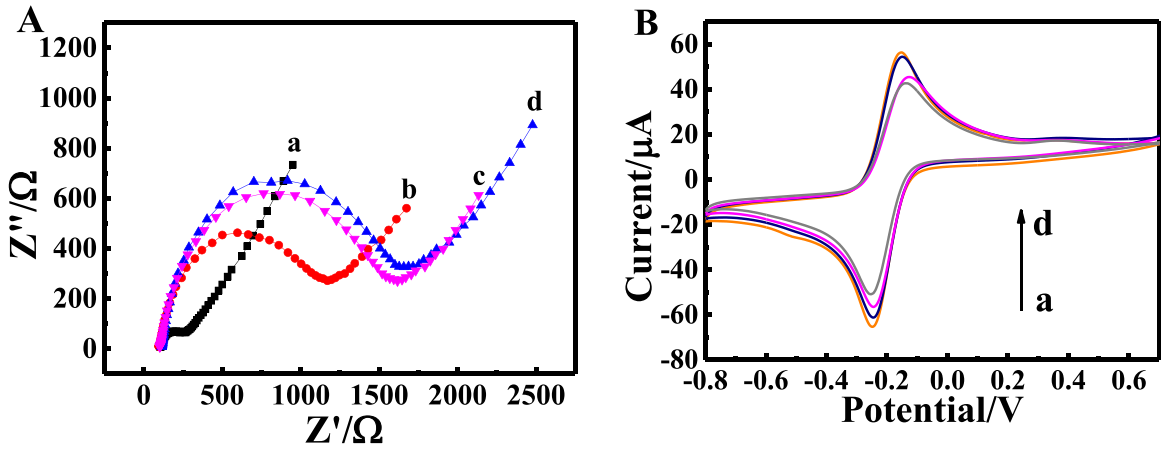


**Fig. 2.** (A) EIS curves and (B) CV curves for the assembled step of the aptasensor in pH 7.4 PBS containing 5 mM $[Fe(CN)_6]^{3-/4-}$. Curves: (a) the bare GCE, (b) AP2/GCE, (c) PDGF-BB/AP2/GCE, (d) ZnS-AP1/PDGF-BB/AP1/GCE.

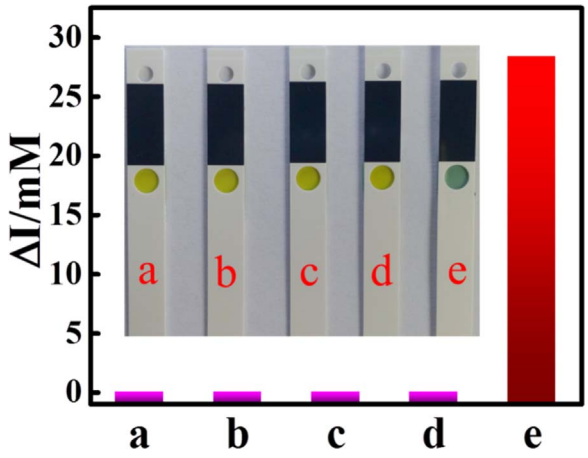


**Fig. 3.** The enhanced signal of the PGM under different conditions: in blank buffer B solution (a); in the resulting assay solution (e) without PDGF-BB (b), AP2 (c), ZnS-AP1(d); Inset in Fig. 3: the corresponding color change of the round control window on the back of the test strip in the experiments. 1.0 M sucrose solution has been added to a different mixture and reacted for 2 h before testing. (For interpretation of the references to color in this figure legend, the reader is referred to the web version of this article.)

AP2 are designed to contain the two PDGF-BB binding aptamers to recognize the PDGF-BB targets. Before the electrode assembly, AP1 was conjugated with ZnS NNC (ZnS-AP1) and the sDNA with thiol and biotin modified at its 3′ and 5′ end were conjugated with invertase and streptavidin-$Fe_3O_4$ NPs, respectively. Initially, the AP2 with thiol modified at 3′ end is self-assembled on GE through Au-S interaction. In the presence of the target PDGF-BB, the ZnS-AP1 is captured on the AP2/GE by the formation of multiple aptamer–protein–aptamer sandwich structures. Subsequent addition of $Ag^+$ triggers the CX reaction to release $Zn^{2+}$ from the ZnS NCCs. The mechanism of CX reaction could be explained that the enthalpy change of the reaction ($ZnS + 2Ag^+ = Zn^{2+} + Ag_2S$) is calculated to be −205.01 kJ (298 K). The CX reaction releases heat, which can happen automatically at room temperature. Each ionic ZnS NCC can release thousands of $Zn^{2+}$ into solution by the CX reaction. After that, the sDNA and 8–17 DNAzyme was added and the produced $Zn^{2+}$ cleaves sDNA in the CAMB system. Because one 8–17 DNAzyme can catalyze the cleavage of several substrates, the CAMB system affords an amplified signal through cycling and regenerating the $Zn^{2+}$-dependent 8–17 DNAzyme to realize multiple enzymatic turnovers. Due to the $Fe_3O_4$ labeled on the one terminal of sDNA, after magnetic separation, the sDNA would be released and the labeled invertase can then convert additional sucrose to glucose, and the final product, glucose, can be detected and quantified by PGM.

Herein, ZnS NCCs play two roles in the system: (1) With large surface areas, ZnS NCCs as labeling tags may be conjugated with a large amount of DNA (AP1) to improve the sensitivity. (2) Through CX reaction, the enclosed cations ($Zn^{2+}$) in ZnS NCCs can be quickly released in a simple and noncorrosive manner for further cleavage in CAMB system. The catalytic and cleavage activities of 8–17 DNAzyme achieved in solution could result in greatly improved stability which could be explained by the fact that enzymes are vulnerable to proteolytic degradation while 8–17 DNAzyme are nucleic acids which have catalytic activity similar to that of enzyme and are more stable and adaptable. Therefore, the portable and triply-amplified detection for the target PDGF-BB was designed with high sensitivity and stability.

### 3.2. Characterization of ZnS NCCs and $Fe_3O_4$ NPs

ZnS NCCs with semihollow core–shell structures were synthesized according to the literature (Yao et al., 2012a, 2012b) and characterized by transmission electron microscopy and X-ray diffractometer. The obtained TEM images of the prepared ZnS NCCs (Fig. 1A) confirmed that, regardless of the particle size, each spherical particle was a cluster of many smaller crystallites (Welch et al., 2014). The clusters exhibits an XRD pattern (Supporting information Fig. S1A), with the main diffraction peaks found to be the (002), (110), and (112) peaks of the pure hexagonal phase of ZnS (JCPDS 36-1450). The (100) and (101) peaks overlapped with the (002) peak because of the peak broadening of (002), typical for small crystallites. To characterize the presence of AP1 on ZnS, FTIR spectra of ZnS (a) and ZnS-AP1 (b) were recorded, which is shown in Fig. S1B. It was obvious that there have been some changes in the FTIR of ZnS with the modification of DNA. Compared with the FTIR of ZnS, the intensity of most bands decreased in curve b which may be due to the conjugation of DNA weakened the peak of ZnS. Moreover, in curve b, the FTIR band appearing at 1090 $cm^{-1}$ is suggested to be associated with the ribose phosphate skeletal motion of DNA molecule, in accordance with the literature's report that $PO^{2-}$ symmetric stretching usually brings a band at 1086 $cm^{-1}$. TEM also confirmed the result. After the conjugation with AP1, the TEM image of ZnS-AP1 (Fig. 1B) changed which showed ZnS NCCs were surrounded by brighter regions, implying the DNA modification may be successful.

The characterization of $Fe_3O_4$ NPs was implemented by means of typical SEM, XRD and UV–vis. As shown in Fig. 1C, $Fe_3O_4$ NPs are spherical with high size uniformity and an average diameter of 150 nm. The crystal structure was determined to be face-centered cubic (View the MathML source) by an XRD pattern (Fig. S2), which is consistent with the literature (Cornell et al., 1996). Fig. 1D shows the SEM images of the $Fe_3O_4$-SA hybrid composites. Compared with the bare $Fe_3O_4$ (Fig. 1C), the $Fe_3O_4$-SA hybrid composites shows aggregated together with a fuzzy view. After further linkage of DNA, the sphere nanopar-

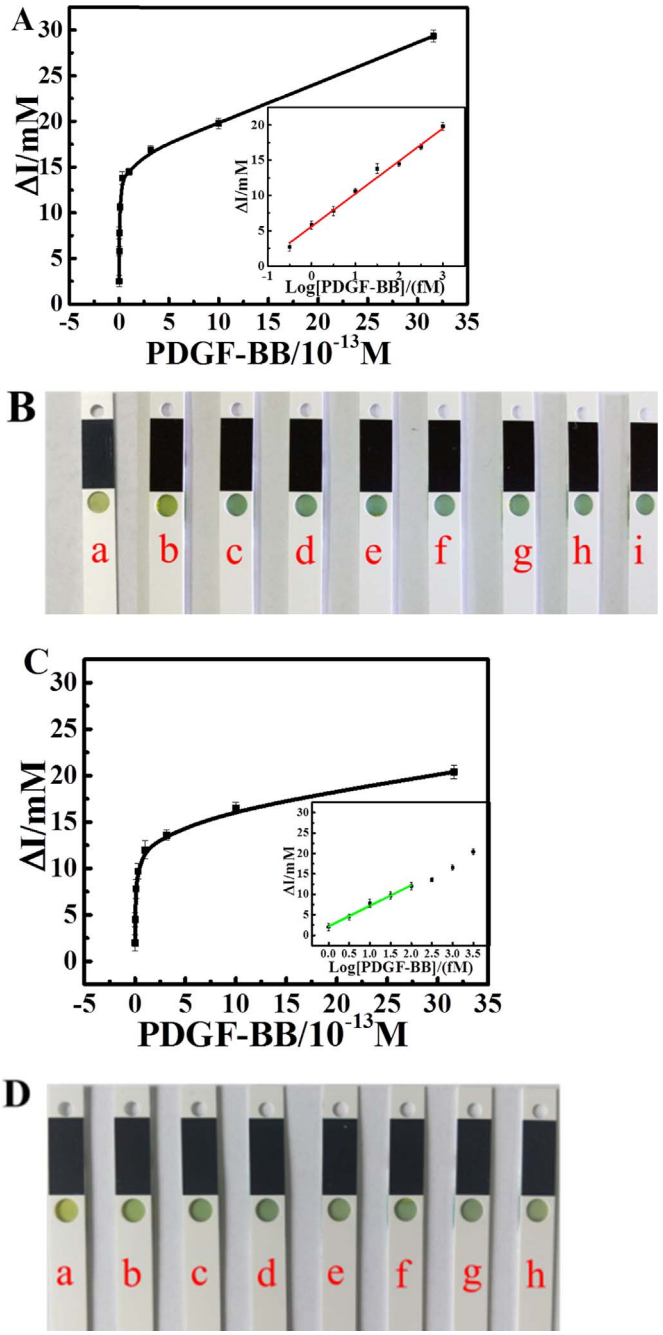


**Fig. 4.** (A) The relationship between the enhanced signal of the PGM and the PDGF-BB concentration and (B) the color change of the round control window on the back of the test strips at different PDGF-BB concentrations. From a to i, the concentrations of PDGF-BB were $3.16\times10^{-16}$ M, $1.0\times10^{-15}$ M, $3.16\times10^{-15}$ M, $1.0\times10^{-14}$ M, $3.16\times10^{-14}$ M, $1.0\times10^{-13}$ M, $3.16\times10^{-13}$ M, $1.0\times10^{-12}$ M, $3.16\times10^{-12}$ M, respectively. The inset in (A) show a calibration curve between the logarithm of PDGF-BB concentrations and the enhanced signal of the PGM. (C) The relationship between the enhanced signal of the PGM and the PDGF-BB concentration in scheme 2 and (D) the color change of the round control window on the back of the test strips at different PDGF-BB concentrations. (For interpretation of the references to color in this figure legend, the reader is referred to the web version of this article.)

ticles were blurred and aggregated even more, shown as Fig. 1E. Furthermore, the characterization of the sDNA-$Fe_3O_4$ by UV–vis was shown in Fig. 1F. No absorption peaks appear in the UV–vis spectrum of $Fe_3O_4$ NPs before they were conjugated with sDNA (curve a). After $Fe_3O_4$ NPs were incubated with sDNA, a new absorption peak at approximately 260 nm, the UV–vis absorption maximum of DNA, was observed in the spectrum of the sDNA-$Fe_3O_4$ solution (curve b). It verifies that the $Fe_3O_4$ NPs have been successfully functionalized with sDNA (Fu and Turro, 1999).

### 3.3. Electrochemical characterization of the modified electrode

Electrochemical impedance spectroscopy provides detailed information about the varied property of surface-modified electrodes for each modification process (Bard et al., 1980). The typical impedance spectrum includes a semicircular portion whose diameter is equal to the electron-transfer resistance, Ret (Armstrong et al., 1986), which reflects the electron transfer kinetics of the redox probe at the electrode surface at higher frequencies (Bard et al., 1980). Fig. 2A showed the characteristic EIS corresponding to the stepwise modification processes. The bare GCE displayed a Ret value of about 300 Ω (curve a). Then, the Ret value obviously increased after AP2 was applied to the electrode surface (1100 Ω) due to it obstructed the electron transfer (curve b). When PDGF-BB, ZnS-AP1 reacted with the electrode, furthermore, the Ret obviously increased to1600 Ω and 1700 Ω (curve c and d), respectively, which may originate from the hydrophobic protein and negative charges DNA sequences blocking the electrode surface.

Different modified electrodes were also studied by CV in $[Fe(CN)_6]^{3-/4-}$ solution. As shown in Fig. 2B, the bare GCE displays a couple of redox peaks originated from the probe of $[Fe(CN)_6]^{3-/4-}$ (curve a). Then the modification of AP2 (curve b), PDGF-BB (curve c), ZnS-AP1 (curve d) step by step on the electrode caused the redox peak current declined gradually because of the lowering electrical conductivity. The EIS and CV results suggested the successful construction of the aptasensor.

### 3.4. The feasibility of the present aptasensor

To demonstrate the feasibility of our new biosensing platform, PGM signal obtained upon analyzing target PDGF-BB and other control experiments were depicted.

Control experiments have been performed to verify the feasibility of the proposed mechanism. The results were summarized in Fig. 3 for buffer B solution (as the blank) (histogram a), PDGF-BB free (histogram b), AP2 free (histogram c) and ZnS-AP1 free (histogram d); the signals from the PGM were low, which indicated that no obvious amount of glucose was generated. This also indicates that the proposed method has a lower background signal. On the contrary, a much higher signal has been detected (histogram e) if the PDGF-BB has been added into the experimental system. In addition, the result of PGM can be estimated by the teststrip via the round colored control window on the back itself. In the above mentioned four control experiments, the sucrose could not be converted into glucose; thus the color did not change (yellow, strips a, b, c and d in the inset). While in the presence of PDGF-BB, sucrose has been converted to glucose by the invertase, which results in color change (green, strip e in the inset). The enhanced PGM signal has some relationship with the concentration of PDGF-BB, which can be applied for quantitative analysis. Therefore, using the PGM for the portable biosensor is feasible.

As shown in Fig. S3, when no $Ag^+$ was present in the system, only a low signal was detected. In addition, control experiments were carried out using the same conditions with PDGF-BB as the model analyte. It was suggested that in the absence of $Ag^+$, $Zn^{2+}$ could not be released from the ZnS NCCs, and the 8–17 DNAzyme could not catalyze the cleavage of the substrate DNA without the $Zn^{2+}$ cofactor. This confirmed the feasibility of our designed assay process.

### 3.5. Optimization of the experimental conditions

The detection sensitivity of the proposed biosensing protocols was influenced by the experimental condition. In order to acquire better assay results, the time of specific recognition between two aptamers

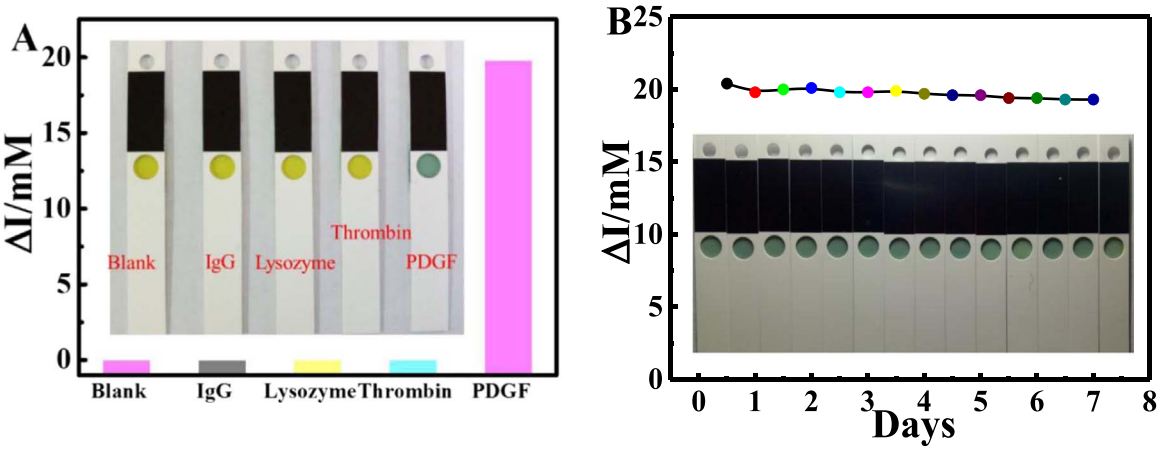


**Fig. 5.** (A)The enhanced signals from the PGM and the inset: the corresponding color of the round control window at different interferents and targets. Concentrations of IgG, lysozyme and thrombin were $1.0\times10^{-10}$ M, and that of PDGF-BB was $1.0\times10^{-12}$ M. The concentration of each probe is 4 mM. (B) stability of the portable aptasensor.

and PDGF-BB has been optimized firstly. As shown in Fig. S4A, with the increase of the reaction time, the detected signals increased sharply at first, and then reached a plateau after 2 h. This indicates that 2 h is enough for the combination of the two aptamers and PDGF-BB, which has been chosen as the optimized condition in the following study.

Furthermore, the effect of enzyme catalysis time on the readout signals has also been studied. The signal of the PGM increases with the increase of the reaction time (Fig. S4B). The reason lies in that more glucose was produced at prolong reaction times. Considering that the detection limit at 20 min is low enough for our system, 20 min has been chosen in this study.

The pH of the solution has a significant effect on the behavior of the aptasensor because the activity of the PDGF-BB and aptamer may be influenced by the highly acidic or alkaline surroundings. In order to optimize the pH, a series of PBS with the pH from 5.0 to 10.0 is prepared. As shown in Fig. S4C, the signal increases initially, reaches a maximum value at a pH of 7.4, and then decreases. Therefore, the optimum pH value for experiment should be about 7.4.

### 3.6. Performance of the portable aptasensor

The signals of the PGM at various concentrations of target under the above optimized conditions are monitored. As shown in Fig. 4A, with the increase of PDGF-BB concentration, the enhanced signal of the PGM increases gradually. The enhanced signal has a good linear relationship with the logarithmic concentration of PDGF-BB in the range of $3.16\times10^{-16}$ M to $1.0\times10^{-12}$ M (see the inset in Fig. 4A), and the regression equation can be expressed as follows: $\Delta I=5.74702+4.57858$ lg C; $R^2=0.99808$, where C is the concentration of PDGF-BB, ΔI is the changing value of the PGM in the presence and absence of PDGF-BB, and R is the regression coefficient. The detection limit is calculated to be 0.11 fM (defined as S/N=3). This detection limit is much lower than the earlier reported aptamer-based colorimetric assay (6 nmol/L) (Chang et al., 2013) and electrochemical aptasensor (63 pmol/L) (Wu et al., 2010). Furthermore, in addition to the signal of the PGM, the colors from the control window changes gradually from yellow to green along with the increasing concentration of PDGF-BB (see Fig. 4B). Thus, the proposed portable aptasensor has a good analytical performance for the detection of PDGF-BB. The analytical performance of the proposed aptasensor has been compared to those previously reported in Table S2. It was plain and clear that our aptasensor showed a better performance than other assays in the analytical range and detection limit. The reason should be taken into account as the employment of 8–17 DNAzyme-aided triply signal amplification which exhibited satisfactory performance as expected.

In addition, in order to prove the triple amplification effect, we compared the present triply amplified with another traditionally amplified portable aptasensor. The design of the traditionally amplified portable aptasensor was shown in Scheme S2. The sandwich aptasensor was prepared by the conjugation of PDGF-BB with AP2 and ZnS-AP1, in which there is no CX and CAMB system. In comparison, as shown in Fig. 4C, the signal of traditionally amplified portable aptasensor also has a high detection limit of 0.33 fM and narrower linear relationship with the logarithmic concentration of PDGF-BB in the range of $1.0\times10^{-15}$ M to $1.0\times10^{-13}$ M (see the inset in Fig. 4C). This result confirms the amplification effect resulting in the great increase in sensitivity of the triply amplified portable aptasensor.

### 3.7. Selectivity, stability and reproducibility of the portable aptasensor

Several proteins (such as IgG, lysozyme, and thrombin) were used as interferences to investigate the selectivity of the portable aptasensor. The concentration of the interferences were settled as $1.0\times10^{-10}$ M and the PDGF-BB concentration was $1.0\times10^{-12}$ M. The enhanced signal of the PGM and the color of the round colored control window were recorded concurrently. As shown in Fig. 5A, nearly no color change in the round colored control window in the presence of interferences has been observed. At the same time, low values were detected by the PGM. On the contrary, in the presence of PDGF-BB, the signal of the PGM has a high value and the color of the control window changes from yellow to green apparently. Compared with the case of PDGF-BB, the effect of these three analog molecules can be ignored. These results suggested that the proposed sensing system was highly selective for the detection of PDGF-BB. Moreover, the stability of the fabricated biosensor was further investigated. It could retain 94.61% of the original value after 7 days consecutive measurements as shown in Fig. 5B. The reproducibility of the as-prepared aptasensor was investigated by prepared seven parallel electrodes under the same conditions. And the relative standard deviation (RSD) was 1.4% for the same concentration of PGDF-BB ($1.0\times10^{-12}$ M), revealing a good reproducibility.

## 4. Conclusions

In summary, a novel triply amplified 8–17 DNAzyme-based portable aptasensor for PDGF-BB detection has been successfully developed. This triply amplified 8–17 DNAzyme-based platform incorporates the CAMB system with CX-based amplification for an ultrasensitive PGM signal, as well as increased stability by its protein enzyme-free design. Moreover, the catalytic and cleavage activities of 8–17 DNAzyme can be achieved in solution; thus, no enzymatic immobiliza-

tion is needed for detection. The quantification of PDGF-BB is relevant to the enhanced signal of the PGM and the change of color in test strips, and 0.11 fM PDGF-BB can be analyzed by this triply amplified strategy. Therefore, given its pocket-size, easy operation, low-cost and wide availability, the proposed portable aptasensor may have wide potential applications in clinical biological analysis and may lead to determination of rapid, online, real time, even employed in personal families.

## Acknowledgments

This work was financially supported by the projects (No. 21005001, 21675001 and 21371007) from National Natural Science Foundation of China, Anhui Provincial Natural Science Foundation (1608085MB46), Anhui Province education department natural sciences key fund (gxyqZD2016023) and Key Program in the Youth Elite Support Plan in Universities of Anhui Province (gxyqZD2016023).

## Appendix A. Supplementary material

Supplementary data associated with this article can be found in the online version at doi:10.1016/j.bios.2017.04.023.

## References

Armstrong, R.D., Lindholm, B., Sharp, M., 1986. J. Electroanal. Chem. Interfacial Electrochem. 202 (1), 69–74.
Bard, A.J., Faulkner, L.R., Leddy, J., 1980. New York: Wiley.
Breaker, R.R., 2000. Science 290, 2095–2096.
Carroll, A.E., Marrero, D.G., Downs, S.M., 2007. Diabetes Technol. Ther. 9, 158–164.
Chang, C.C., Wei, S.C., Wu, T.H., Lee, C.H., Lin, C.W., 2013. Biosens. Bioelectron. 42, 119–123.
Clark, L.C., Lyons, C., 1962. Ann. N.Y. Acad. Sci. 102, 29–45.
Clarke, M.F., Westin, E., Schmidt, D., Joseph's, S.F., Ratner, L., Gallo, R.C., Reitz, M.S.J., 1984. Nature 308, 464–467.
Cornell, R.M., Schwertmann U., 1996. New York.
Daar, A.S., Thorsteinsdóttir, H., Martin, D.K., Smith, A.C., Nast, S., Singer, P.A., 2002. Nat. Genet. 32, 229–232.
Deng, H., Li, X.L., Peng, Q., Wang, X., Chen, J.P., Li, Y.D., 2005. Angew. Chem. Int. Ed. 18, 2842–2845.
Fan, C., Plaxco, K.W., Heeger, A.J., 2005. Trends Biotechnol. 23, 186–192.
Favier, F., Walter, E.C., Zach, M.P., Benter, T., Penner, R.M., 2001. Science 293, 2227–2231.
Fu, P.K.L., Turro, C., 1999. J. Am. Chem. Soc. 121, 1–2.
Giepmans, B.N.G., Adams, S.R., Ellisman, M.H., Tsien, R.Y., 2006. Science 312, 217–224.
Jiang, H., Zhang, X.J., Wang, G.F., 2015. Biosens. Bioelectron. 74, 931–938.
Kucuur, E., Boldt, F.M., Cavaliere-Jaricot, S., Ziegler, J., Nann, T., 2007. Anal. Chem. 79, 8987.
Li, J.S., Schachermeyer, S., Wang, Y., Yin, Y.D., Zhong, W.W., 2009a. Anal. Chem. 81, 9723–9729.
Li, J., Zhang, T., Ge, J., Yin, Y., Zhong, W., 2009b. Angew. Chem. Int. Ed. 48, 1588–1591.
Liu, J., Cao, Z., Lu, Y., 2009. Chem. Rev. 109, 1948–1998.
Lu, L., Zhang, X., Kong, R., Yang, B., Tan, W., 2011. J. Am. Chem. Soc. 133, 11686–11691.
Ma, X.M., Chen, Z.H., Zhou, J., Weng, W., Zheng, O., Lin, Z.Y., Guo, L.H., Qiu, B., Chen, G.N., 2014. Biosens. Bioelectron. 55, 412–416.
Martinez, A.W., Phillips, S.T., Butte, M.J., Whitesides, G.M., 2007. Angew. Chem. Int. Ed. 46, 1318–1320.
Montagnana, M., Caputo, M., Giavarina, D., Lippi, G., 2009. Clin. Chim. Acta 402, 7–13.
Murray, R.W., 2008. Chem. Rev. 108, 2688–2720.
Peng, X., Wickham, J., Alivisatos, A.P., 1998. J. Am. Chem. Soc. 120, 5343–5344.
Pierce, G.F., Tarpley, J.E., Tseng, J., Bready, J., Chang, D., Kenney, W.C., Rudolph, R., Robson, M.C., Berg, J.V., Reid, P., 1995. J. Clin. Investig. 96 (3), 1336–1350.
Qiu, L.P., Wu, Z.S., Shen, G.L., Yu, R.Q., 2011. Anal. Chem. 83 (8), 3050–3057.
Robertson, D.L., Joyce, G.F., 1990. Nature 344, 467–468.
Shi, Y.P., Zhang, H., Yue, Z.F., Zhang, Z.M., Teng, K.S., Li, M.J., Yi, C.Q., Yang, M.S., 2013. Nanotechnology 24 (37), 375501.
Su, J., Xu, J., Chen, Y., Xiang, Y., Yuan, R., Chai, Y.Q., 2013. Biosens. Bioelectron. 45, 219–222.
Tang, L.H., Liu, Y., Ali, M.M., Kang, K.D., Zhao, W.A., Li, J.H., 2012. Anal. Chem. 84 (11), 4711–4717.
Wang, W.J., Li, J.J., Rui, K., Gai, P.P., Zhang, J.R., Zhu, J.J., 2015. Anal. Chem. 87, 3019–3026.
Wang, F., Han, Y., Lim, C.S., Lu, Y.H., Wang, J., Xu, J., Chen, H.Y., Zhang, C., Hong, M.H., Liu, X.G., 2010. Nature 463, 1061–1065.
Wegner, S.V., Okesli, A., Chen, P., He, C., 2007. J. Am. Chem. Soc. 129, 3474–3475.
Welch, M.E., Ritzert, N.L., Chen, H., Smith, N.L., Tague, M.E., Xu, Y., Baird, B.A., Abruña, H.D., Ober, C.K., 2014. J. Am. Chem. Soc. 136, 1879–1883.
Wilson, D.S., Szostak, J.W., 1999. Annu. Rev. Biochem. 68, 611–647.
Wu, Z.S., Zhou, H., Zhang, S.B., Shen, G.L., Yu, R.Q., 2010. Anal. Chem. 82 (6), 2282–2289.
Xia, F., Zuo, X.L., Yang, R.Q., Xiao, Y., Kang, D., Vallée-Bélisle, A., Gong, X., Yuen, J.D., Hsu, B.B.Y., Heeger, A.J., Plaxco, K.W., 2010. Proc. Natl. Acad. Sci. 107, 10837–10841.
Xiang, Y., Lu, Y., 2013. Chem. Commun. 49 (6), 585–587.
Xiang, Y., Lu, Y., 2012a. Anal. Chem. 84 (9), 4174–4178.
Xiang, Y., Lu, Y., 2012b. Anal. Chem. 84 (4), 1975–1980.
Xiang, Y., Lu, Y., 2011. Nat. Chem. 3 (9), 697–703.
Yan, L., Zhu, Z., Zou, Y., Huang, Y.S., Liu, D.W., Jia, S.S., Xu, D.M., Wu, M., Zhou, Y., Zhou, S., Yang, C.Y., 2013. J. Am. Chem. Soc. 135 (10), 3748–3751.
Yao, J.J., Han, X.G., Zeng, S., Zhong, W.W., 2012a. Anal. Chem. 84, 1645–1652.
Yao, J., Flack, K., Ding, L., Zhong, W., 2013. Analyst 138, 3121–3125.
Yao, J., Han, X., Zeng, S., Zhong, W., 2012b. Anal. Chem. 84, 1645–1652.
Yao, J., Schachermeyer, S., Yin, Y., Zhong, W., 2011. Anal. Chem. 83, 402–408.
Zhang, J., Campbell, R.E., Ting, A.Y., Tsien, R.Y., 2002. Nat. Rev. Mol. Cell Biol. 3, 906–918.
Zhang, L., Yang, C.L., Zhao, G.Y., Mu, J.S., Wang, Y., 2015a. Sens. Actuators B 210, 190–196.
Zhang, S.B., Hu, X., Yang, X.H., Sun, Q.L., Xu, X.L., Liu, X.W., Shen, G.Y., Lu, J.L., Shen, G.L., Yu, R.Q., 2015b. Biosens. Bioelectron. 66, 363–369.
Zhang, X.B., Kong, R.M., Lu, Y., 2011. Annu. Rev. Anal. Chem. 4, 105–128.
Zhang, X.B., Wang, Z., Xing, H., Xiang, Y., Lu, Y., 2010. Anal. Chem. 82, 5005–5011.
Zhang, X.R., Liu, H.X., Li, R.J., Zhang, N.B., Xiong, Y., Niu, S.Y., 2015c. Chem. Commun. 51, 6952–6955.
Zhang, Z., Zhang, C., 2012. Anal. Chem. 84 (3), 1623–1629.
Zhou, Z., Xiang, Y., Tong, A., Lu, Y., 2014. Anal. Chem. 86, 3869–3875.